Supplementary Information

Experimental Section

Chemicals

$RuCl_3$, $FeCl_3$, $NaNO_3$, NaH_2PO_2, HCl and acetonitrile were purchased from Sinopharm Chemical. The solvent in the experiment was deionized water.

Preparation of Ru-modified FeOOH and Ru-modified FeP

First, 5 mg $RuCl_3$ and 50 mg FeOOH (The preparation of FeOOH was reported by previous paper.[1]) were dispersed in 50 mL deionized water, and were stirring vigorously for 24 h at room temperature. The resultant samples were collected by washing with DI water three times, and then dried at 80 ℃ for 24 h in vacuum oven. The obtained Ru-modified FeOOH powder and NaH_2PO_2 (Fe: P = 1: 5, molar ratio) was put in a porcelain boat, where NaH_2PO_2 was put at the upstream side. Then, the samples were heated to 300 ℃ and maintained for 2 h in the Ar flow, the flow rate of Ar was 30 ml/min and the heating rate was 2 ℃/min. Ru-modified FeP was collected after cooled to ambient temperature.

Characterization

The XRD patterns were characterized in Bruker D8 Advance X-ray diffractometer (10 °/min). The X-ray diffractometer possess monochromatized Cu Kα radiation, λ= 1.5406Å, tube current, 40 mA and tube voltage, 40 mV. The powder of Ru-modified FeP can be used directly for XRD test. TEM images were conducted in JEOL JEM-2100F electron microscopy, the operate voltage was 200 kV. Furthermore, the JEOL ARM-200 microscope was used to characterize the HAADF-STEM images and EDS elemental mapping, the accelerating voltage was 300 kV. Before the TEM characterizations, the catalyst was dispersed into the ethanol to form a homogeneous suspension, which was then used for TEM characterizations. The X-ray photoelectron spectra (XPS) analysis was performed on Thermo escalab 250XI. The Thermo

escalab 250XI instrument is equipped with an Al Kα source (hν= 1486.6 eV). The binding energy scale of all measurements was calibrated by referencing C 1s to 284.8 eV.The Agilent ICPOES730 was used for the inductively coupled plasma optical emission spectrometry (ICP-OES). The concentration of Ru atom was directly measured by ICP-OES.

Electrochemical measurements

We conducted the electrochemical measurements in a three-electrode cell. Typically, the homogeneous ink was prepared by mixing the sample (4mg), Nafion solution (0.05 wt%, 10uL) with 1ml water-isopropanol solution (1:1, volume ratio) through sonicating. Subsequently, a certain volume of the suspension was dropped onto the surface of glassy carbon electrode to make the catalyst loading of 0.408 mg cm^{-2}. The HER polarization curve was conducted in H_2-saturated 0.5 M H_2SO_4 electrolyte with a scan rate of 5 mV s^{-1}. The working electrode was the glassy carbon electrode (5mm in diameter), the counter electrode was graphite rod and the Hg/Hg_2Cl_2 (in 3 M KNO_3 solution) electrode was the reference electrode. All potentials measured were calibrated vs RHE using the following equation: $E_{RHE} = E_{Hg/Hg_2Cl_2} + 0.0592 \times PH + 0.242$

The uncompensated ohmic resistance (R) was measured by the iR compensation function of the workstation. The iR correction was conducted as $E_{corr} = E–iR$, where E was the applied overpotential, and i was the current density. All potentials used has been converted to the reversible hydrogen electrode (RHE).

The turnover frequency (TOF) value was calculated according to the previous report,[2, 3] and the detail was described as below:

$$TOF = \frac{Total\ hydrogen\ turnovers\ per\ geometric\ area}{Active\ sites\ per\ geometric\ area}$$

The total number of hydrogen turn overs was calculated from the current density according to:

$$\#_{H^2} = \left(j\frac{mA}{cm^2}\right)\left(\frac{1C/s}{1000\ mA}\right)\left(\frac{1\ mol\ e^-}{96485.3\ C}\right)\left(\frac{1\ mol\ H_2}{2\ mol\ e^-}\right)\left(\frac{6.02 \times 10^{23}\ molecules\ H_2}{1\ mol\ H_2}\right)$$
$$= 3.12 \times 10^{15}\ \frac{H_2/s}{cm^2}\ per\ \frac{mA}{cm^2}$$

The upper limit of the number of active sites was calculated based on the hypothesis that all Ru atoms in the Ru-modified FeP catalyst formed active Ru(+3)-P_4-Fe centers and all of them were accessible to the electrolyte. The real number of active sites were twice the accessible Ru sites and should be considerably lower than the calculated value. The bulk Ru content of Ru-modified FeP revealed by the ICP-OES measurement was 0.95 wt%. Accordingly, the upper limit of active Ru site density is:

$$\frac{0.95}{100} \times \frac{mg}{mg} \times 0.408 \frac{mg}{cm^2} \times \frac{1}{101.07} \times \frac{mmol}{mg} \times 6.022 \times 10^{20} \frac{sites}{mmol}$$
$$= 2.31 \times 10^{16} sites\ cm^{-2}$$

the upper limit of active site density is: $4.62 \times 10^{16} sites\ cm^{-2}$

For example, at an overpotential of 100 mV, the HER current density is 22.2 mA cm^{-2}, and the TOF of the Ru-modified FeP was calculated to be

$$\text{TOF} = \left(\frac{3.12 \times 10^{15} \frac{H_2/s}{cm^2} per \frac{mA}{cm^2} \times 22.2 \frac{mA}{cm^2}}{4.62 \times 10^{16} sites\ cm^{-2}} \right) = 1.50\ s^{-1}$$

Similarly, the TOF value of Ru-modified FeP at an overpotential of 200 mV was calculated to be

$$\text{TOF} = \left(\frac{3.12 \times 10^{15} \frac{H_2/s}{cm^2} per \frac{mA}{cm^2} \times 34.8 \frac{mA}{cm^2}}{4.62 \times 10^{16} sites\ cm^{-2}} \right) = 2.35\ s^{-1}$$

The faradaic efficiency is calculated based on the equation: $\eta = znF/Q$. where η is the faradaic efficiency of hydrogen, z is the number of electrons required to form a molecule of H_2, n is the measured amount of product (mol), F is the Faraday constant (96,500 C mol^{-1}), Q is the quantity of electricity consumption.

Ex-situ XAFS measurements

We used the Shanghai Synchrotron Radiation Facility (SSRF, BL14W1 station, operated at 3.5 GeV with a maximum current of 250 mA) to perform the Ru K-edge X-ray absorption data. The samples were placed in an aluminum sample holder, and then the data was collected in the mode of fluorescence. We use the first peak maximum of the first derivative of a Ru foil (22117 eV) to calibrate the energy. The spectra for references were collected in the mode of transmission. The data obtained were all performed at room temperature.

We used the Beijing Synchrotron Radiation Facility (BSRF, BL1W1B station, operated at 2.5 GeV with a maximum current of 250 mA) to perform the Fe K-edge X-ray absorption data. The samples were placed in an aluminum sample holder, and then the data was collected in

the mode of fluorescence. We use the first peak maximum of the first derivative of a Fe foil (7112 eV) to calibrate the energy. The spectra for references were collected in the mode of transmission. The data obtained were all performed at room temperature.

Operando Electrochemical XAS Measurements

The operando experiments were performed in orgonic glass electrochemical cell. A single circular hole of 1.5 cm in the flat walls establish a link between the electrolyte and the catalyst. The side of carbon cloth with Ru-modified FeP coating faced inward. The coated carbon cloth was connected with the electrochemical workstation through a slip of copper. Before the experiment, we poured H_2SO_4 electrolyte into the cell. The reference electrode fixed by the orgonic glass cap was used for the entire experiment to make the distance between working and reference electrode constant. The homogeneity of the materials was measured by recording at different positions of the coated carbon cloth. The Ru K-edge (BL14W1 in SSRF) and the Fe K-edge (BL1W1B in BSRF) spectra were recorded at the same electrodes. Spectra were recorded on the dry Ru-modified FeP films at first and then in H_2SO_4 solution at open circuit potential and -80 mV vs RHE. We recorded five spectrums at Ru K-edge and three spectrums at Fe K-edge, at each potential. Before transfer to the next potential, the system enabled to restore balance for 20 min. Results identified that the spectra recorded at a given potential was no noticeable change.

XAFS Data Analysis

The acquired EXAFS data were processed according to the standard procedures using the Athena and Artemis implemented in the IFEFFIT software packages. The fitting detail is described below:

The acquired EXAFS data were processed according to the standard procedures using the ATHENA module implemented in the IFEFFIT software packages. The EXAFS spectra were obtained by subtracting the post-edge background from the overall absorption and then normalizing with respect to the edge-jump step. Subsequently, the $\chi(k)$ data of were Fourier

transformed to real (R) space using a hanning windows (dk=1.0 Å^{-1}) to separate the EXAFS contributions from different coordination shells. To obtain the quantitative structural parameters around central atoms, least-squares curve parameter fitting was performed using the ARTEMIS module of IFEFFIT software packages.[4]

The following EXAFS equation was used:

$$\chi(k)=\sum_j \frac{N_j S_o^2 F_j(k)}{k R_j^2}\exp[-2k^2\sigma_j^2]\exp[\frac{-2R_j}{\lambda(k)}]\sin[2kR_j+\phi_j(k)]$$

S_0^2 is the amplitude reduction factor, $F_j(k)$ is the effective curved-wave backscattering amplitude, N_j is the number of neighbors in the j^{th} atomic shell, R_j is the distance between the X-ray absorbing central atom and the atoms in the j^{th} atomic shell (backscatterer), λ is the mean free path in Å, $\phi_j(k)$ is the phase shift (including the phase shift for each shell and the total central atom phase shift), σ_j is the Debye-Waller parameter of the j^{th} atomic shell (variation of distances around the average R_j). The functions $F_j(k)$, λ and $\phi_j(k)$ were calculated with the ab initio code FEFF8.2. The coordination numbers of model samples were fixed as the nominal values. The obtained S_0^2 was fixed in the subsequent fitting. While the internal atomic distances R, Debye-Waller factor σ^2, and the edge-energy shift ΔE_0 were allowed to run freely.

Computational Method

Density Functional Theory calculations were performed as the framework of the first-principle simulation. Interaction between electrons and nuclei was described by the projector augmented wave (PAW) pseudo-potentials.[5] A cut-off energy of 480 eV was selected through the calculations. The k-point was chosen to be 2 × 4 × 2 grid with a gamma point for the bulk calculations, and 4 × 1 × 1 for surface calculations. The global break condition for the electronic self-consistency loop is 1.0e^{-5} eV. Hubbard-U (U=5.3) correction is applied for Fe as the d-band correction.[6-8] The relaxation of ions will stop if the largest force is smaller than

0.02 eV/ Å. Transition state energy is calculated with the Nudged Elastic Band (NEB) method with 3 inserted images. The global break condition for the NEB calculations is 0.05 eV/ Å.[9]

The detail of DFT calculations

1) Free Energy of Adsorbate for Electrochemical Hydrogen evolution reaction (HER)

The adsorption free energy of H, ΔG_{H*} is calculated to evaluate the electrochemical activity of HER. It is shown as below,

$$\Delta G_{H*} = G_{H*} - G_{*} - \frac{1}{2} G_{H^2} \quad (1)$$

where G_{H*} and G_{*} are the Gibb's free energies of the adsorbed H atom on the catalytic surface and the empty surface. G_{H^2} is the Gibb's free energies of gas phase H2 molecule, which is calculated in a large supercell. The Gibb's free energy of adsorbate is calculated as,

$$\Delta G = \Delta E + \Delta \mathrm{ZPE} - T\Delta S + \Delta G_{\mathrm{U}} + \Delta G_{\mathrm{pH}} \quad (2)$$

in which ΔE is the reaction energy derived from Density Functional Theory (DFT) calculation, ΔG_{U} is the change of the applied potential, ΔG_{pH} is the change of the pH value. $\Delta \mathrm{ZPE}$ is the change of zero-point energy before and after the adsorption, which is calculated from vibrational frequencies as the following equation:

$$ZPE = \sum_i^{N_{modes}} ZPE^i = \sum_i^{N_{modes}} \frac{1}{2} h\upsilon_i \quad (3)$$

ΔS is the change of entropy upon adsorption of the intermediate. However, the adsorbate on the surface is considered to have an entropy of 0, because the adsorbate loses all its translational and rotational degrees of freedom. Thus, ΔS is calculated as,

$$\Delta S_{ads} = S_{ads} - S_{gas-phase} = -S_{gas-phase} = k_B \ln(1 - e^{\frac{-h\upsilon_i}{k_B T}}) \quad (4)$$

k_B is the Boltzmann constant. T is the operating temperature which is the room temperature (300K) in this case, and h is the Planck constant.

2) Reaction pathways of Electrochemical Hydrogen evolution reaction (HER)

For a typical electrochemical HER process, three reaction pathways may occur during reaction condition, which are Volmer, Tafel and Heyrovsky steps. In this work, we used DFT to calculate the reaction free energy and reaction barrier of Volmer, Heyrovsky and Tafel steps written as below,

Volmer: $\mathrm{H}^+ + e^- + * = H^*$ (5)

Heyrovsky: $H^* + H^+ + e^- = H_2 + *$ (6)

Tafel: $H^* + H^* = H_2 + *$ (7)

The reaction free energies are calculated as,

$$\Delta G_{Volmer} = G_{H*} - \frac{1}{2} G_{H_2} - G_*$$

$$\Delta G_{Heyrovsky} = G_{H_2} + G_* - G_{H*} - \frac{1}{2} G_{H_2}$$

$$\Delta G_{Tafel} = G_{H_2} + G_* - 2 * G_{H*}$$

Figures and tables

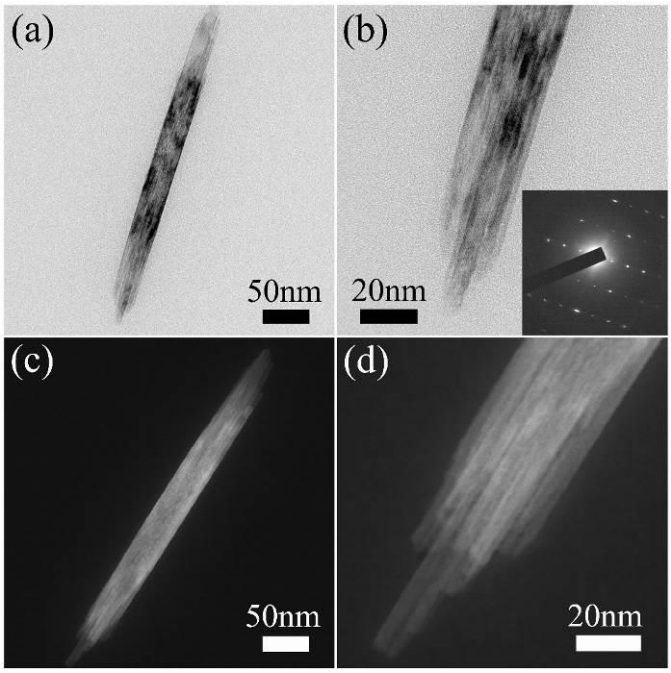

Fig. S1. The TEM characterizations of the isolated single atom Ru-modified FeOOH nanorods. The SAED pattern indicates that the as-prepared Ru-modified FeOOH nanorods are well crystalline.

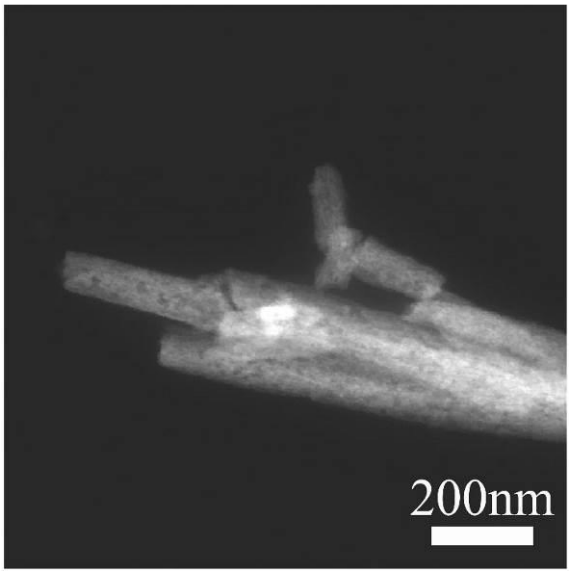

Fig. S2. The TEM images of the isolated single atom Ru-modified FeP. The TEM images show that the Ru-modified FeP roughly remain the rod-like shape, but the surfaces become extremely bumpy, due to the redox reaction during the phosphatizing process.

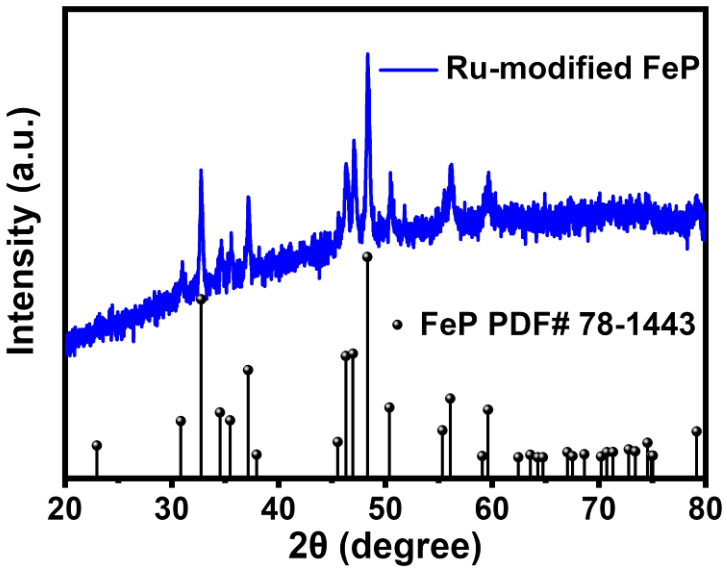

Fig. S3. The XRD patterns of the isolated single atom Ru-modified FeP. The X-ray powder diffraction (XRD) pattern for the Ru-modified FeP correspond to FeP (JCPDS No. 78-1443).

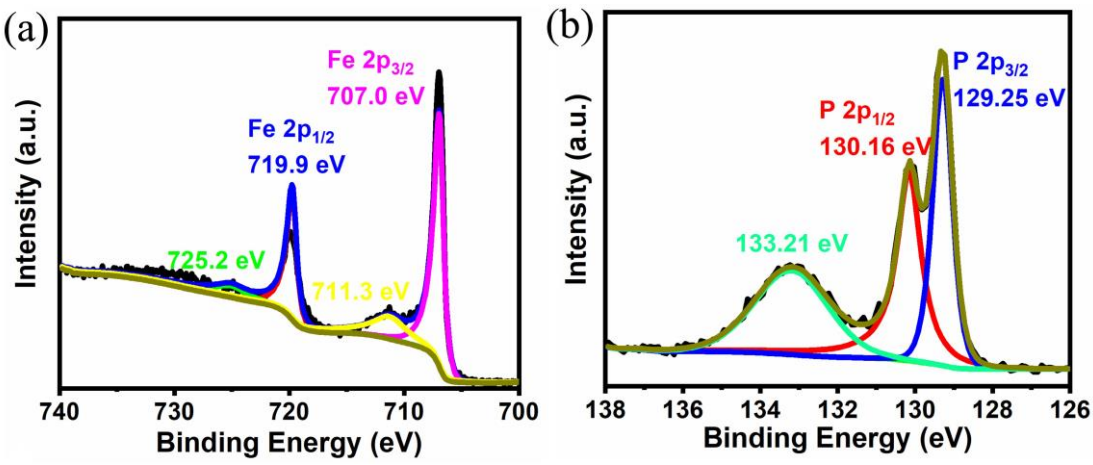

Fig. S4. XPS spectra in (a) Fe 2p and (b) P 2p regions for isolated single atom Ru-modified FeP.

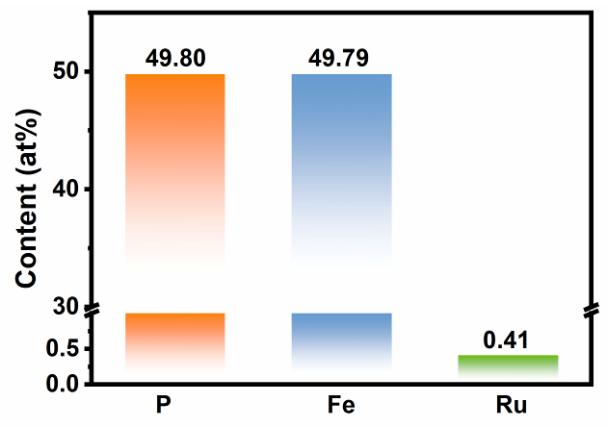

Fig. S5. The atomic content percentages of P, Fe and Ru in Ru-modified FeP measured by ICP-OES analysis.

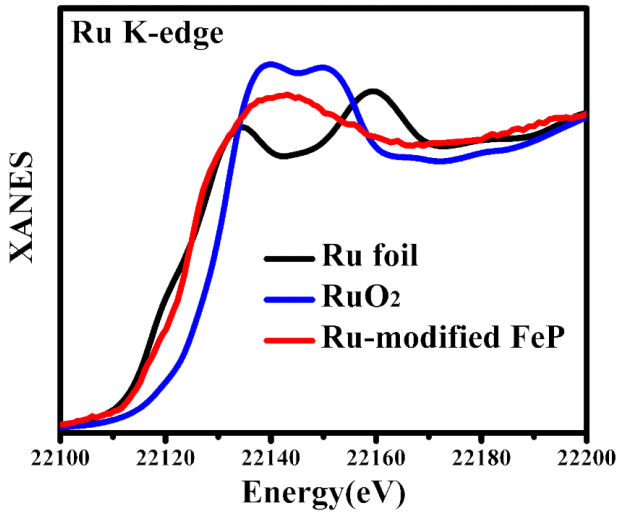

Fig. S6. The XANES curves of Ru K-edge for isolated single atom Ru-modified FeP. Herein, Ru foil and RuO_2 are used as standard references.

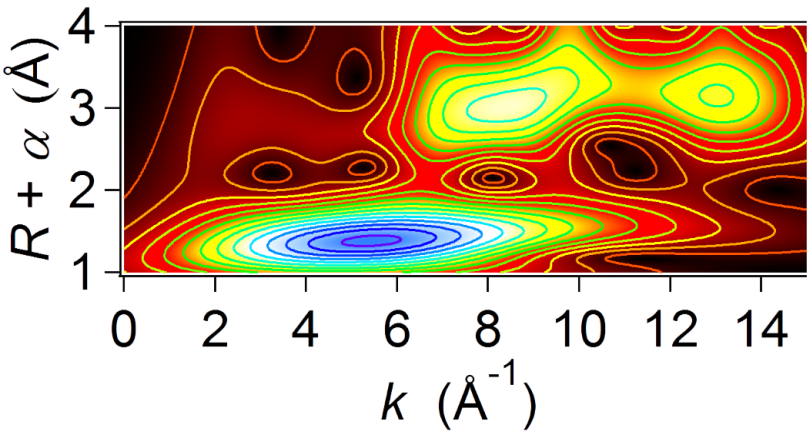

Fig. S7. WT plot of the RuO_2. In EXAFS analysis, the FT magnitude of experimental data provides resolution in the radial distance of neighbouring scatterers. However, the information is lost at the wave number *k* at which the scatterer contributes. Since the position in *k*-space is related to the atomic species of the backscattering atom, important information is lost in the magnitude of the transformed signal. So it is necessary to develop new methods for the analysis of EXAFS, such as WT, which has powerful resolution in both *k* and *R* spaces. WT is thought to be a wonderful supplement for FT.

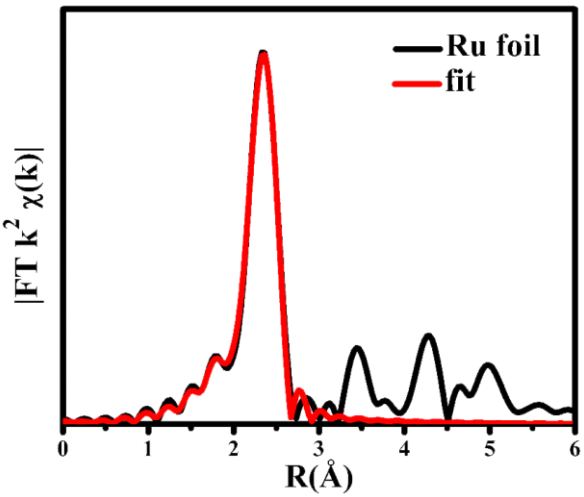

Fig. S8. FT-EXAFS fitting curves of the Ru foil at Ru K-edge.

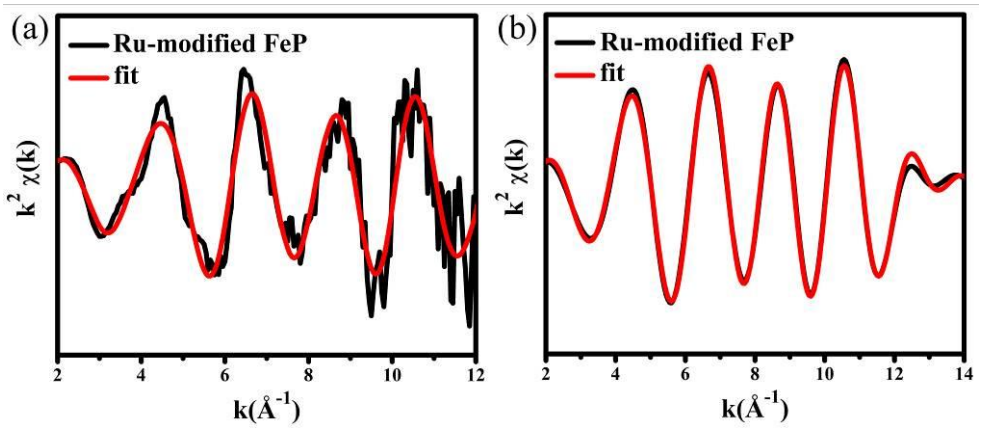

Fig. S9. (a) The *k* space EXAFS fitting curve of isolated single atom Ru-modified FeP at Ru K-edge. (b) The inversed FT-EXAFS fitting curve of Ru-modified FeP at Ru K-edge. Qualitatively, the available information from the EXAFS oscillation is the amplitude, the frequency, and the phase. To a first approximation, amplitude is proportional to coordination number, while frequency is inversely related to bond length. The phase of the EXAFS and the shape of the amplitude envelope provide information about the scatterer.

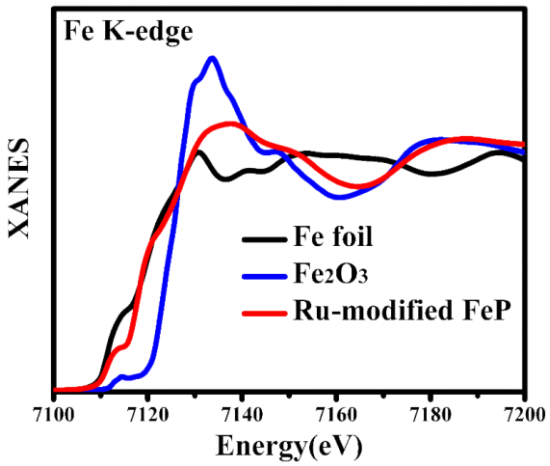

Fig. S10. XANES curves of Fe K-edge for isolated single atom Ru-modified FeP. The oxidation state of Fe are reflected through the absorption threshold of the XANES curves. The position of Ru-modified FeP situated between Fe foil and Fe_2O_3, indicating the oxidation state of Fe species in Ru-modified FeP was between the two references.

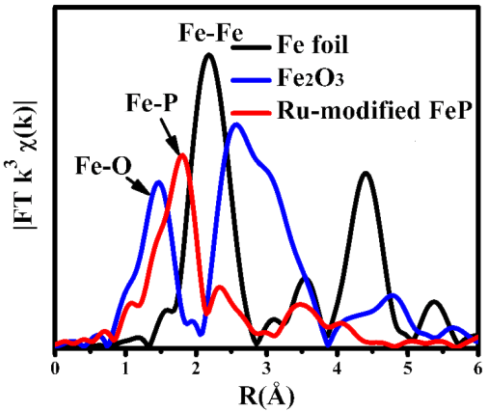

Fig. S11. EXAFS curves of Fe K-edge for Ru-modified FeP. The FT peak of Fe-P in Ru-modified FeP, Fe-O in Fe_2O_3 and Fe-Fe in Fe foil is centered at 1.81 Å, 1.46 Å and 2.19 Å, respectively.

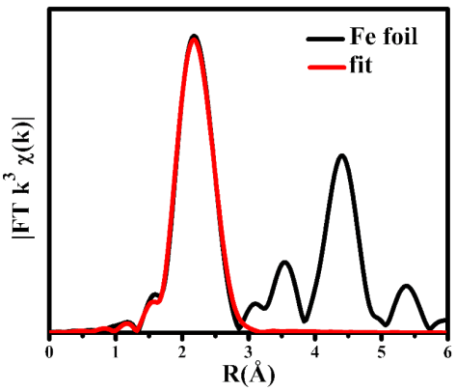

Fig. S12. FT-EXAFS fitting curves of the Fe foil at Fe K-edge. The obtained S_0^2 was 0.75.

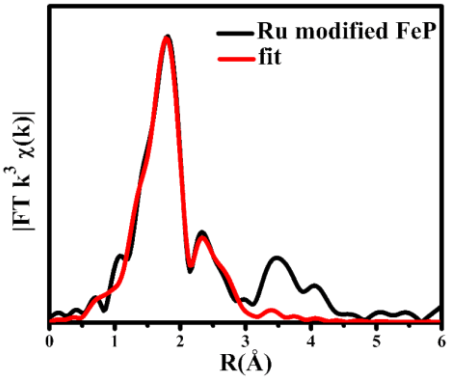

Fig. S13. FT-EXAFS fitting curves of the Ru-modified FeP at Fe K-edge.

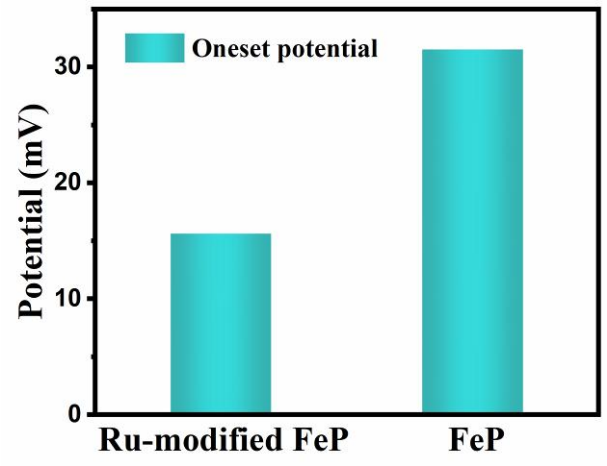

Fig. S14. The calculated oneset potential for Ru-modified FeP and FeP.

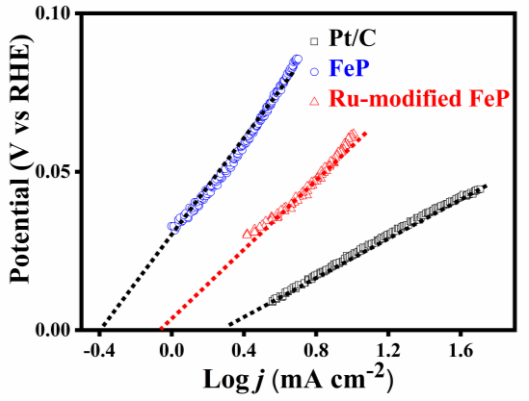

Fig. S15. Calculated exchange current density in 0.5 M H_2SO_4 by applying extrapolation method to the Tafel plot.

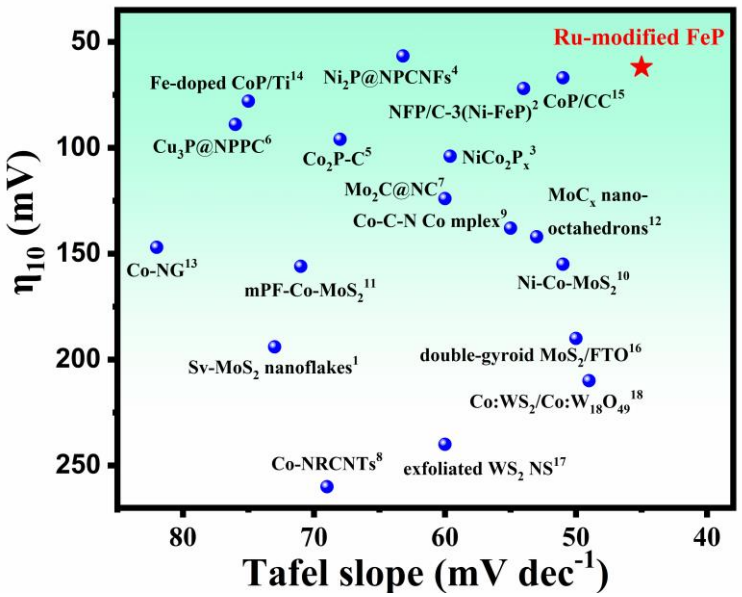

Fig. S16. Comparison of HER performance between isolated single atom Ru-modified FeP and other electrocatalysts in acidic media.

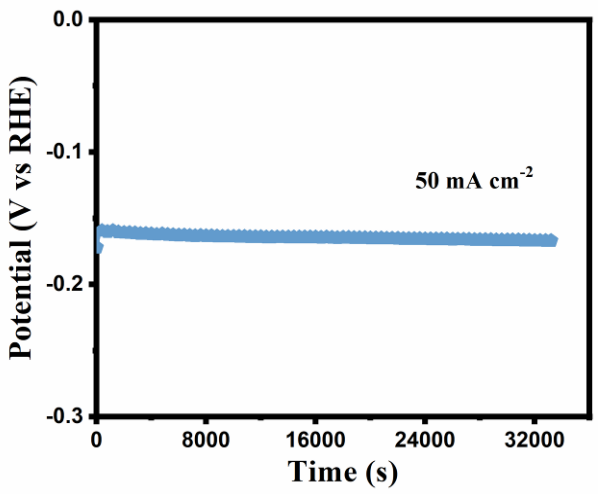

Fig. S17. The chronopotentiometric curve at the current density of 50 mA cm^{-2}.

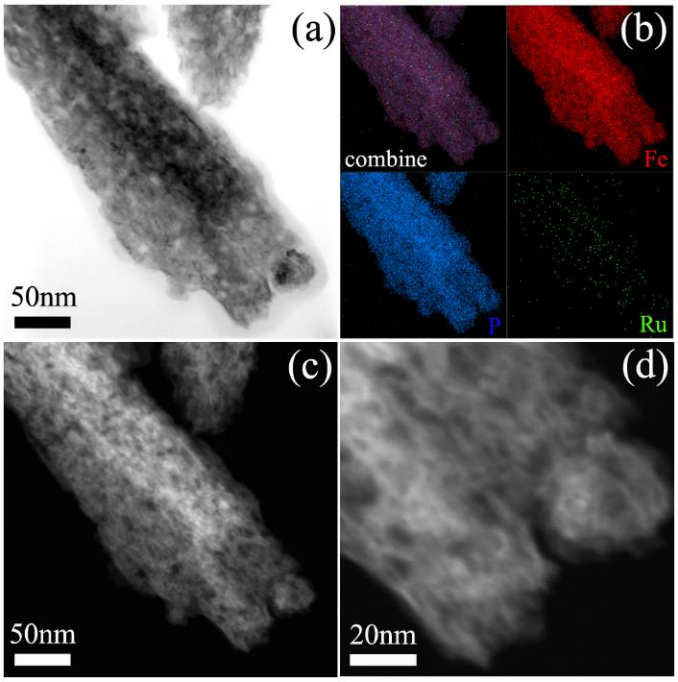

Fig. S18. TEM images and EDS mappings of the isolated single atom Ru-modified FeP after HER.

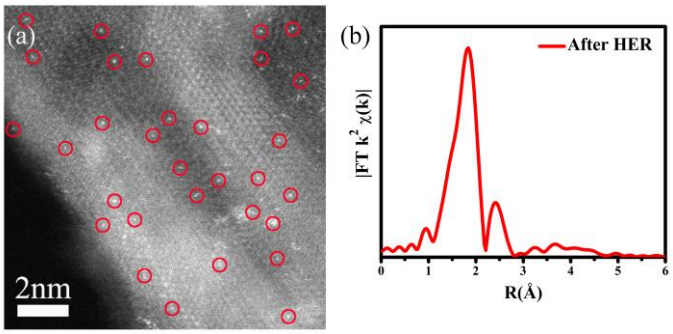

Fig. S19. (a) The HAADF-STEM image of the isolated single atom Ru-modified FeP after HER cycles. (b) The Ru K-edge EXAFS curve of the Ru-modified FeP after HER cycles.

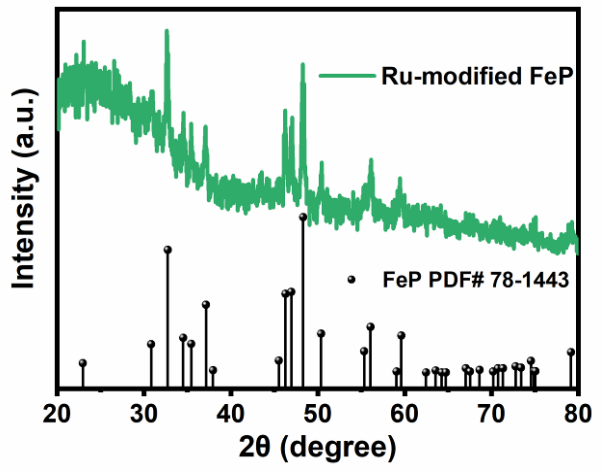

Fig. S20. The XRD patterns of the isolated single atom Ru-modified FeP after catalysis.

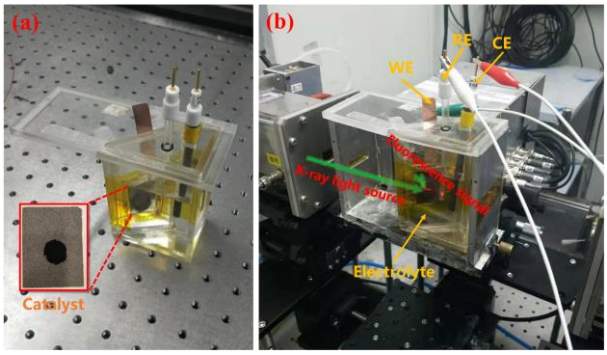

Fig. S21. The detail of the operando X-ray absorption spectroscopy measurement. The device is set up at BL1W1B with the support from BSRF, where the X-ray induced fluorescence model is applied. CE, counterelectrode; WE, working electrode; RE, reference electrode.

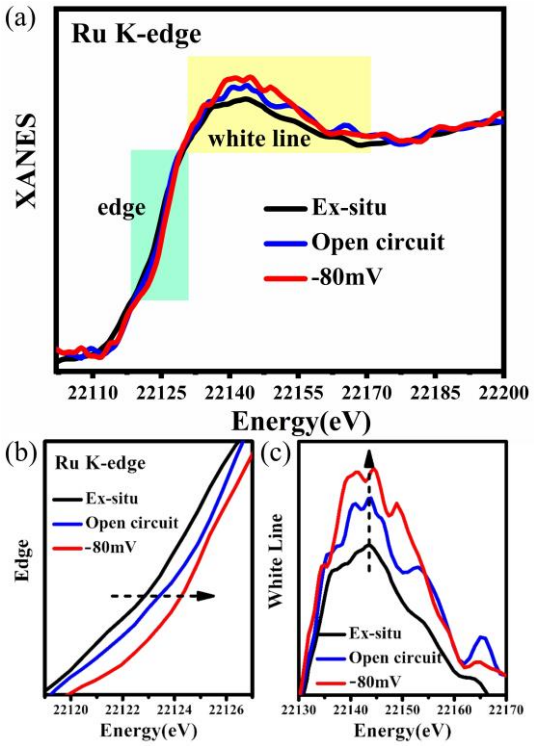

Fig. S22. (a) Ru K-edge XANES spectra of Ru-modified FeP during HER. (b) The absorption edge evolution and (c) the white line peak evolution of Ru-modified FeP at Ru K-edge under operando XAS condition.

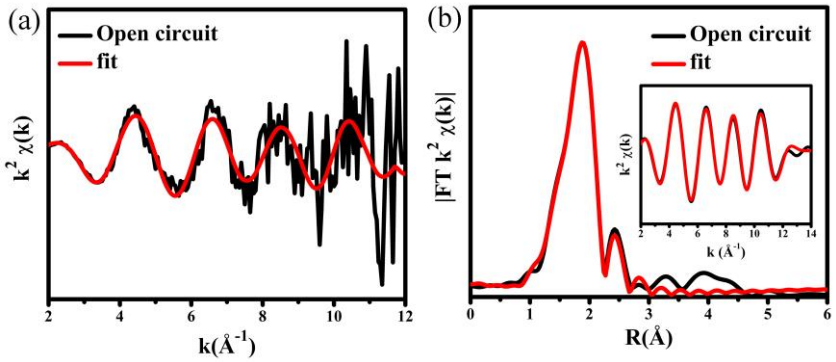

Fig. S23. (a) The Ru K-edge *k* space EXAFS and (b) FT-EXAFS fitting curve of the Ru-modified FeP at open circuit potential. The inset is the corresponding Ru K-edge inversed FT-EXAFS fitting curve.

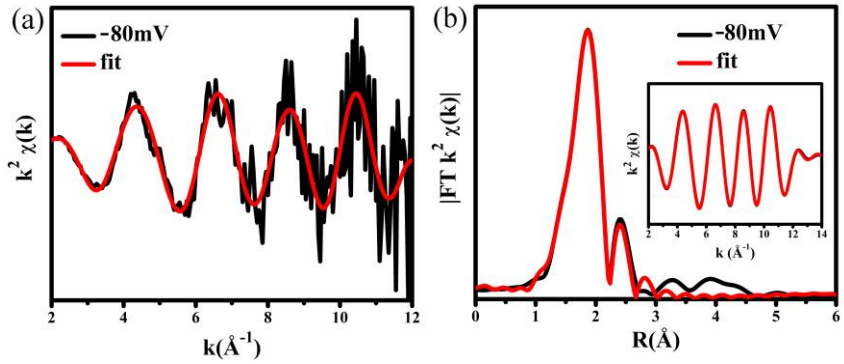

Fig. S24. (a) The Ru K-edge *k* space EXAFS and (b) FT-EXAFS fitting curve of the Ru-modified FeP at -80 mV. The inset is the corresponding Ru K-edge inversed FT-EXAFS fitting curve.

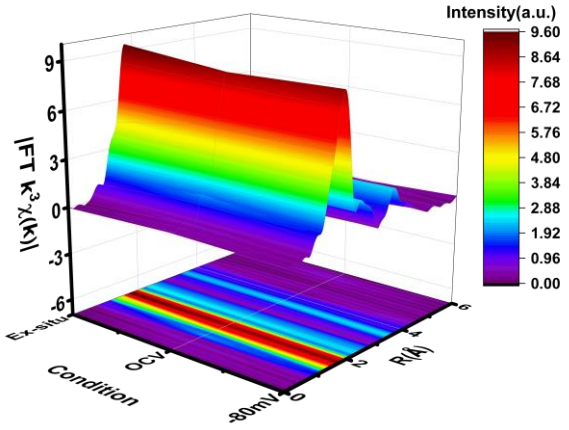

Fig. S25. (b) k^3-weighted Fe K-edge FT-EXAFS spectra of Ru-modified FeP during HER.

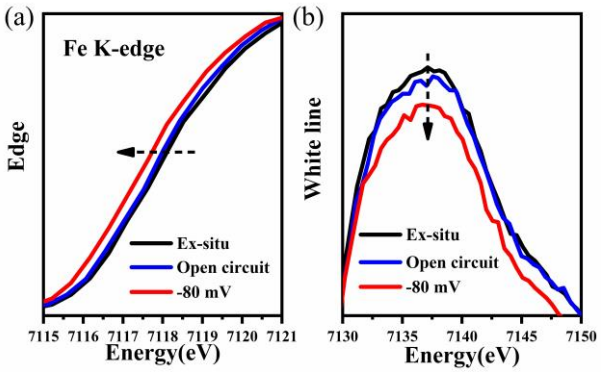

Fig. S26. (a) The absorption edge evolution and (b) the white line peak evolution of Ru-modified FeP at Fe K-edge under operando XAS condition

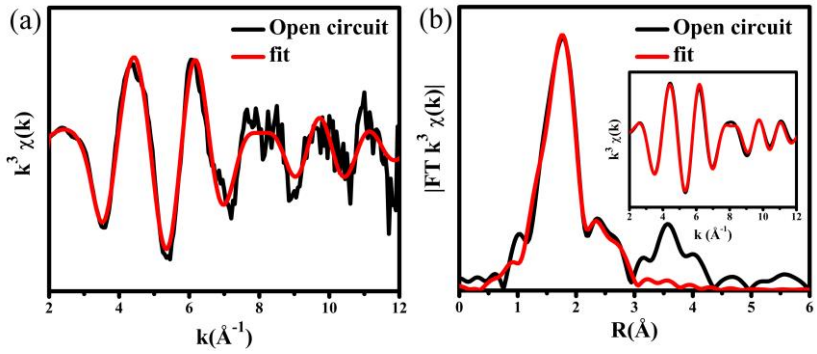

Fig. S27. (a) The Fe K-edge *k* space EXAFS and (b) FT-EXAFS fitting curve of the Ru-modified FeP at open circuit potential. The inset is the corresponding Fe K-edge inversed FT-EXAFS fitting curve.

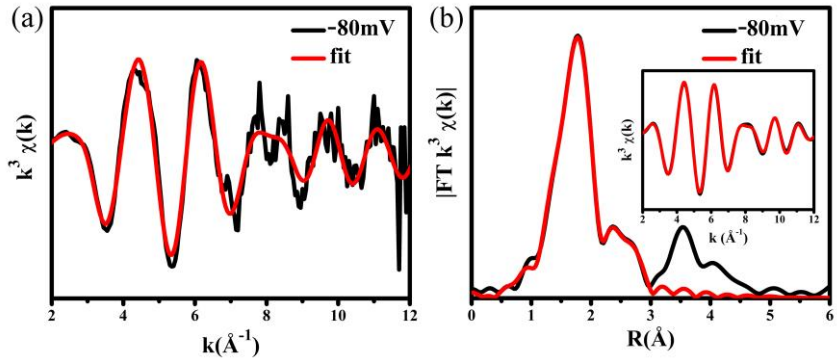

Fig. S28. (a) The Fe K-edge *k* space EXAFS and (b) FT-EXAFS fitting curve of the Ru-modified FeP at -80 mV. The inset is the corresponding Fe K-edge inversed FT-EXAFS fitting curve.

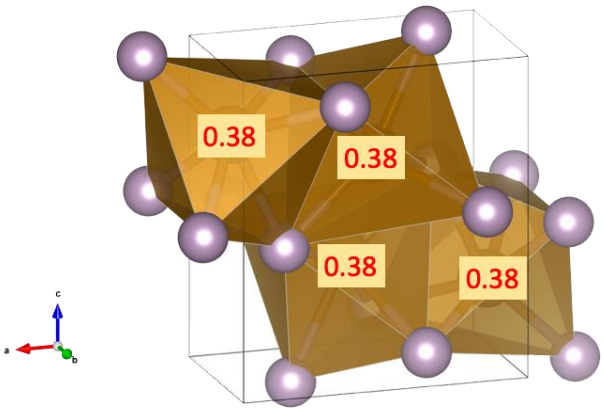

Fig. S29. Pnma bulk structure of Fe_4P_4. Numbers are magnetic moments of the Fe atoms indicating the ferromagnetic ordering. Brown is the Fe octohedral, and purple is the P atom.

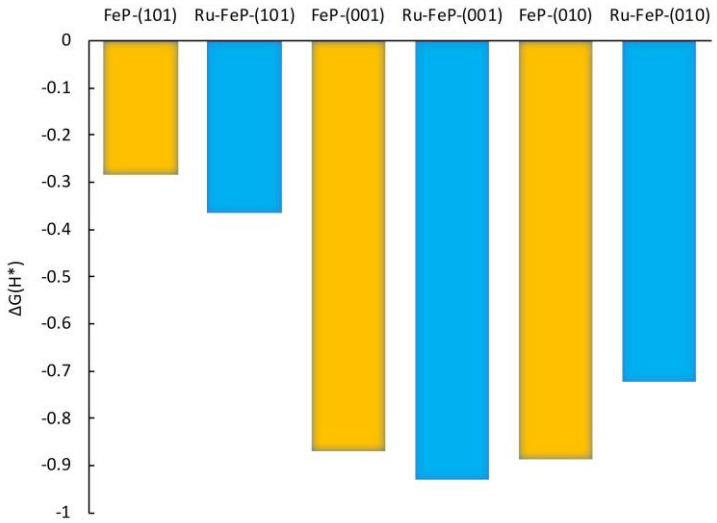

Fig. S30. Free energy of hydrogen adsorption (ΔG_{H^*}) for all Ru-modified FeP and FeP systems.

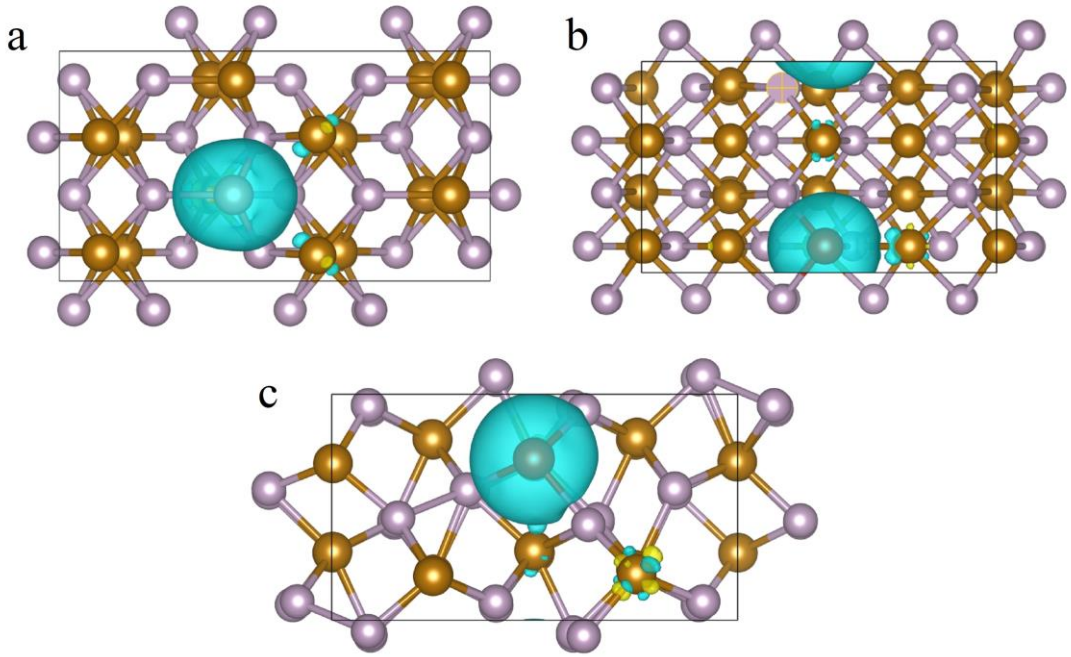

Fig. S31. Charge density difference analysis for (a) (010), (b) (001) and (c) (101) surfaces.

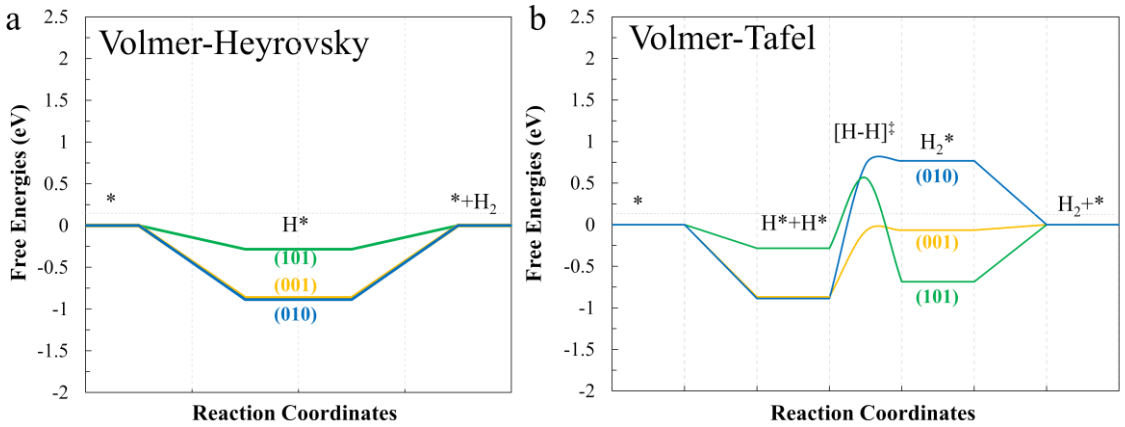

Fig. S32. Energy diagrams of (a) Volmer-Heyrovsky and (b) Volmer-Tafel steps for FeP-(010), FeP-(001) and FeP-(101) systems.

Table S1. Structural parameters extracted from the Ru K-edge EXAFS fitting. (S_0^2=0.86).

Sample	***Scattering pair***	***CN***	***R(Å)***	***σ^2(10^{-3}Å^2)***	***ΔE_0(eV)***	***R factor***
Ru-modified FeP	Ru-P	4.3±0.5	2.37±0.01	4.5±0.5	1.5±0.5	0.003
	Ru-Fe	1.7±0.6	2.76±0.01	5.2±0.7		
Ru foil	Ru-Ru_1	6*	2.64±0.01	3.2±0.4	2.0±0.5	0.006
	Ru-Ru_2	6*	2.72±0.01	3.5±0.4		

Table S2. Structural parameters extracted from the Fe K-edge EXAFS fitting. (S_0^2=0.75).

Sample	***Scattering pair***	***CN***	***R(Å)***	***σ^2(10^{-3}Å^2)***	***ΔE_0(eV)***	***R factor***
Ru-modified FeP	Fe-P	6.0±0.6	2.26±0.01	5.2±0.5	1.5±0.5	0.004
	Fe-Fe	4.1±0.5	2.65±0.01	6.2±0.6		
Fe foil	Fe-Fe_1	8*	2.47±0.01	6.5±0.5	0.5±0.4	0.005
	Fe-Fe_2	6*	2.84±0.01	7.2±0.4		

For the EXAFS fitting in Tables S1-S2 and S4-S5, S_0^2 is the amplitude reduction factor; CN is the coordination number; R is interatomic distance (the bond length between Ru central atoms and surrounding coordination atoms); σ^2 is Debye-Waller factor (a measure of thermal and static disorder in absorber-scatterer distances); ΔE_0 is edge-energy shift (the difference between the zero kinetic energy value of the sample and that of the theoretical model). R factor is used to value the goodness of the fitting.

* This value was fixed during EXAFS fitting, based on the known structure of Ru foil and Fe foil.

Error bounds that characterize the structural parameters obtained by EXAFS spectroscopy were estimated as N ± 20%; R ± 1%; σ^2 ± 20%; ΔE_0 ± 20%.

Table S3. Comparison of HER performance between isolated single atom Ru-modified FeP and other electrocatalysts in acidic media.

NO.	***Catalyst***	***Tafel slope (mV dec^{-1})***	***Current density (j, mA/cm2)***	***η at the corresponding j (mV)***	***Reference***
	Ru-modified FeP	**45**	**1**	**15.6**	**This work**
			10	**62**	
1	Sv-MoS_2 nanoflakes	73	10	194	*Angew. Chem.* **2019**, *131*, 2051.
2	NFP/C-3(Ni-FeP)	54	10	72	*Sci. Adv.* **2019**, *5*, 2.
3	$NiCo_2Px$	59.6	10	104	*Adv. Mater.* **2017**, *29*, 1605502.
4	Ni_2P@NPCNFs	63.2	10	56.7	*Angew. Chem.* **2018**, *130*, 1981.
5	Co_2P-C	68	10	96	*J. Am. Chem. Soc.* **2017**, *139*, 11248.
6	Cu_3P@NPPC	76	10	89	*Adv. Mater.* **2018**, *30*, 1703711.
			20	117	
			80	307	
7	Mo_2C@NC	60	10	124	*Angew. Chem. Int. Ed.* **2015**, *54*, 10752.
8	Co-NRCNTs	69	10	260	*Angew. Chem. Int. Ed.* **2014**, *53*, 4372.
9	Co-C-N Co mplex	55	10	138	*J. Am. Chem. Soc.* **2015**, *137*, 15070.
10	Ni-Co-MoS_2	51	10	155	*Adv. Mater.* **2016**, *28*, 9006
11	mPF-Co-MoS_2	71	10	156	*Nat. Commun.* **2017**, *8*, 14430.
12	MoCx nano-octahedrons	53	1	87	*Nat. Commun.* **2015**, *6*, 6512.
			10	142	
13	Co-NG	82	10	147	*Nat. Commun.***2015**, ***6***, 8668.
14	Fe-doped CoP/Ti	75	10	78	*Adv. Mater.* **2017**, *29*, 1602441.
15	CoP/CC	51	10	67	*J. Am. Chem. Soc.* **2014**, *136*, 7587-7590.
			20	100	
16	double-gyroid MoS_2/FTO	50	2	190	*Nature Mater.* **2012**, *11*, 963-969.
17	exfoliated WS_2 NS	60	10	240	*Nature Mater.* **2013**, *12*, 850-855.
18	Co:WS_2/Co:$W_{18}O_{49}$	49	10	210	*Energy Environ. Sci.* **2018**, *11*, 2270-2277

Table S4. Structural parameters extracted from the Ru K-edge EXAFS fitting. (S_0^2=0.86).

Sample	*Scattering pair*	*CN*	*R(Å)*	*$\sigma^2(10^{-3}Å^2)$*	*ΔE_0(eV)*	*R factor*
Ru-modified FeP at OCV	Ru-P	4.2±0.5	2.41±0.01	4.9±0.4	2.5±0.5	0.004
	Ru-Fe	1.9±0.4	2.76±0.01	5.8±0.5		
Ru-modified FeP at -80mV	Ru-P	4.3±0.6	2.43±0.01	5.1±0.7	2.5±0.5	0.005
	Ru-Fe	1.7±0.5	2.77±0.01	5.4±0.6		

Table S5. Structural parameters extracted from the Fe K-edge EXAFS fitting. (S_0^2=0.75).

Sample	***Scattering pair***	***CN***	***R(Å)***	***σ^2(10^{-3}Å^2)***	***ΔE_0(eV)***	***R factor***
Ru-modified FeP at OCV	Fe-P	5.9±0.6	2.26±0.01	5.3±0.5	2.0±0.4	0.005
	Fe-Fe	3.9±0.4	2.64±0.01	5.7±0.7		
Ru-modified FeP at -80mV	Fe-P	5.8±0.5	2.26±0.01	4.8±0.8	2.0±0.4	0.006
	Fe-Fe	4.0±0.6	2.65±0.01	6.1±0.6		

Table S6. Information of the unit cell for DFT models.

	X (Å)	Y (Å)	Z (Å)	α (°)	β (°)	γ (°)
FeP-(010)	6.101	11.493	25.786	90	90	90
FeP-(001)	6.101	10.315	28.731	90	90	90
FeP-(101)	10.315	6.506	24.406	117.964	90	90

References

1. P. Jiang, Q. Liu, Y. Liang, J. Tian, A. M. Asiri, X. Sun, *Angew. Chem., Int. Ed.* 2014, **53**, 12855-12859.

2. J. Yin, J. Jin, M. Lu, B. Huang, H. Zhang, Y. Peng, P. Xi and C.-H. Yan, *J. Am. Chem. Soc.* 2020, DOI: 10.1021/jacs.0c05050.

3. H.-W. Liang, S. Bruller, R. Dong, J. Zhang, X. Feng & K Mullen, *Nat. Commun.* 2020, **6**, 7992.

4. B. Ravel, M. Newville, *J. Synchrotron Rad.* 2005, **12**, 537-541.

5. P. E. Blöchl, *Phys. Rev. B: Condens. Matter Mater. Phys.* 1994, **50**, 17953-17979.

6. A. Jain, G. Hautier, S. P. Ong, C. J. Moore, C. C. Fischer, K. A. Persson, G. Ceder, *Phys. Rev. B: Condens. Matter Mater. Phys.* 2011, **84**, No. 045115.

7. D.-H. Seo, A. Urban, G. Ceder, *Phys. Rev. B: Condens. Matter Mater. Phys.* 2015, **92**,115118;

8. S. W. Kim, D. H. Seo, X. H. Ma, G. Ceder, K. Kang, *Adv. Energy Mater.* 2012, **2**, 710-721.

9. G. Henkelman, B. P. Uberuaga, H. A Jónsson, *J. Chem. Phys.* 2000, **113**, 9901-9904.